ACS APPLIED MATERIALS & INTERFACES

Research Article

www.acsami.org

Cobalt Oxide-Carbon Nanosheet Nanoarchitecture as an Anode for High-Performance Lithium-Ion Battery

Huanlei Wang,*[,†] Nan Mao,[†] Jing Shi,[†] Qigang Wang,[‡] Wenhua Yu,[†] and Xin Wang*[,†]

[†]Institute of Materials Science and Engineering, Ocean University of China, Qingdao 266100, China

[‡]Department of Chemistry and Advanced Research Institute, Tongji University, Shanghai 200092, China

Supporting Information

ABSTRACT: To improve the electrochemical performance of cobalt oxide owing to its inherent poor electrical conductivity and large volume expansion/contraction, Co_3O_4-carbon nanosheet hybrid nanoarchitectures were synthesized by a facile and scalable chemical process. However, it is still a challenge to control the size of Co_3O_4 particles down to ~5 nm. Herein, we created nanosized cobalt oxide anchored 3D arrays of carbon nanosheets by the control of calcination condition. The uniformly dispersed Co_3O_4 nanocrystals on carbon nanosheets held a diameter down to ~5 nm. When tested as anode materials for lithium-ion batteries, high lithium storage over 1200 mAh g^{-1} is achieved, whereas high rate capability with capacity of about 390 mAh g^{-1} at 10 A g^{-1} is maintained through nanoscale diffusion distances and interconnected porous structure. After 500 cycles, the cobalt oxide-carbon nansheets hybrid display a reversible capacity of about 970 mAh g^{-1} at 1 A g^{-1}. The synergistic effect between nanosized cobalt oxide and sheetlike interconnected carbon nanosheets lead to the greatly improved specific capacity and the initial Coulombic efficiency of the hybrids.

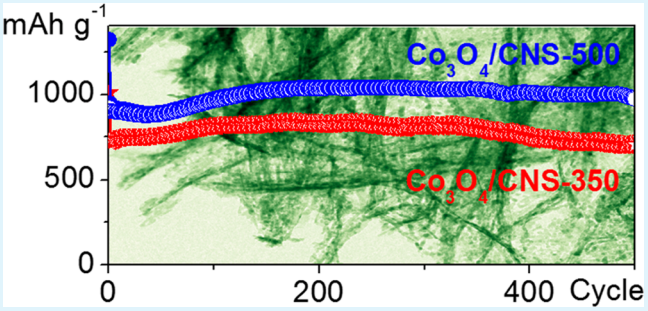

KEYWORDS: *electrochemistry, cobalt oxide, Li-ion battery, anode, hybrid, energy storage*

INTRODUCTION

Lithium-ion batteries have achieved great success in electricity storage and supply.[1] The main challenges in this field are achieving high reversible capacity, stable cycle performance and excellent rate capability for suitable electrode materials.[2−5] Thus, various electrochemically active materials made of carbon, metal, metal oxide, and sulfide have been recently designed for enhanced lithium storage. In particular, transition metal oxide is considered as a promising anode candidate as a result of the advantages associated with its high theoretical capacity, environmental friendliness, and low cost.[4] Among these transition metal oxides, Co_3O_4 has received a particular interest as one of the most promising anodes due to its high theoretical capacity of 890 mAh g^{-1}. Unfortunately, transition metal oxides suffer from poor cycling performance and low rate capability due to large specific volume changes upon cycling and sluggish kinetic of both electron and lithium-ion transport.

To circumvent the poor cycle and high-rate problems of transition metal oxides, tremendous efforts have been made to improve its electrochemical performance by optimizing the size of particles,[6,7] coating with electronically conductive layers,[8−10] and constructing a three-dimensional conducting networks.[11,12] In this respect, a variety of carbonaceous materials, including porous carbons,[13] carbon aerogels,[11] carbon nanofibers,[14,15] carbon nanotubes,[16,17] and graphene,[12,18,19] have been utilized for the incorporation of metal oxides. Graphene with high electrical conductivity, good flexibility, and high chemical stability has been widely used to support metal oxides, which facilitates electron transport and Li^+ diffusion of anchored host materials. Graphene-based hybrid materials exhibit enhanced lithium storage,[20,21] but the synthesis process of high-quality graphene is still complicated. Recently, metal oxide nanoparticles embedded in porous carbon nanofibers have been successful synthesized by a low-cost electrospinning technique which also exhibited improved specific capacity and rate capability.[14,15] However, the controllable synthesis of nanosized metal oxides is still a challenge.

Recently, graphene-like carbon nanosheets were successfully achieved by using biomass, which is a cost-effective approach to create value-added materials.[22] The obtained partially graphitic 3D arrays of 2D carbon nanosheets exhibit high surface area and good electrical conductivity, which are different from conventional biomass-derived activated carbons. Such low-cost carbon nanosheet shows great potential in the substitution of graphene materials, which can be used as conducting networks to support metal oxides with controlled size. Here, we demonstrate an efficient strategy to large-scale fabrication of carbon nanosheet-supported cobalt oxide hybrid architectures. The resulting hybrid architectures retained most of the structural properties of carbon nanosheets, such as high conductivity, and

Received: November 22, 2014
Accepted: January 9, 2015
Published: January 9, 2015

DOI: 10.1021/am508208c
ACS Appl. Mater. Interfaces 2015, 7, 2882−2890

interconnected porous structure, which can not only facilitate easy access of the electrolyte ions into the electrode and ensure fast diffusion of electrons, but also can prevent the aggregation of metal oxides and accommodate the volume change during cycling process. As a result, the carbon nanosheets-cobalt oxide hybrid nanoarchitectures can achieve high reversible capacity, superior rate capability, and excellent cycling performance, thus exhibiting great potential as an anode material for lithium storage.

EXPERIMENTAL SECTION

Synthesis of Co_3O_4-carbon nanosheet hybrid. Similar to that previously reported, carbon nanosheets were synthesized by combined hydrothermal carbonization and chemical activation techniques using hemp bast fiber as the precursor.[22] The resultant carbon nanosheets were denoted as CNS. The CNS assemblies were first treated with 50 wt % HNO_3 at 60 °C for 4 h.[13] $CoCl_2{\cdot}6H_2O$ (0.25 mmol) and urea (1.25 mmol) were added to 100 mL of water, followed by the addition of 20 mg of acid-treated CNS. Subsequently, the mixture was refluxed under stirring at 120 °C for 6 h. After cooling to room temperature, the composites were washed with deionized water and dried at 60 °C. Finally, the samples were heated at 350 or 500 °C for 5h under an argon atmosphere. The obtained composites were labeled as Co_3O_4/CNS-*T*, where *T* represents the calcination temperature. Bare Co_3O_4 was prepared as above-described without the addition of CNS.

Characterization. The X-ray diffraction (XRD) was carried out on a Bruker D8 Discover diffractometer using Cu Kα radiation. The morphology of the composite was examined by filed-emission scanning electron microscopy (SEM). Transmission electron microscopy (TEM) was conducted with a JEOL JEM-2010 microscope operated at 200 kV. Thermogravimetric analysis (TGA, PerkinElmer TGA 4000) was measured with a heating rate of 5 °C min^{-1} under 200 mL min^{-1} of flowing air. X-ray photoelectron spectroscopy (XPS) analysis was conducted with an ULTRA (Kratos Analytical) spectrometer equipped with Al K_α X-ray source. Fourier transform infrared spectra (FTIR) were acquired using Nicolet 8700 spectrometer in the range of 4000−400 cm^{-1}. Raman spectroscopy analysis was performed with a confocal microprobe Raman system (Thermo Nicolet Almega XR Raman Microscope). The measurement of the nitrogen adsorption−desorption isotherms was done with a Quantachrome Autosorb-1 at −196 °C.

Electrochemical Measurements. Electrochemical performance was evaluated via CR2032-type coin cell on a computer controlled Land Battery Measurement System (CT2001A) at various current densities of 0.1 A g^{-1} to 10 A g^{-1} in the fixed voltage range of 3−0.01 V vs. Li/Li^+ at room temperature. The working electrode was composed of 80 wt % active material, 10 wt % acetylene black (Super P), and 10 wt % poly(vinylidene fluoride) (PVDF) binder dissolved in *N*-methyl-2-pyrrolidinone (NMP). The loading density of the electrodes ranged from 0.6 to 1.0 mg cm^{-2}. The coin cells were fabricated inside an Ar filled glovebox using Li metal as the counter electrode, polyethene separator, and 1.0 M $LiPF_6$ in 1:1 (volume ratio) ethylene carbonate:dimethyl carbonate (EC/DMC) as the electrolyte.

RESULTS AND DISCUSSION

The overall synthetic procedure for Co_3O_4/CNS composite is illustrated in Scheme 1. During hydrolysis, urea uniformly releases hydroxyl ions in the mixture, which results in the precipitation of hydroxides.[23] The hydrophilic functional groups on the highly porous carbon nanosheet act as anchoring sites for the precipitates. Finally, the precipitates are converted into metal oxides after calcination. Notably, the weight fractions of cobalt oxide in the as-prepared hybrid architecture determined from TGA is about 49.5 wt % (Figure S1, Supporting Information), which can be controlled by adjusting the ratios between the metal salts and the CNS. Both advantages of nanoscale cobalt oxide and sheet-like interconnected carbon

Scheme 1. Schematic Illustration of the Formation of Carbon Nanosheet-Supported Co_3O_4 Nanocrystals

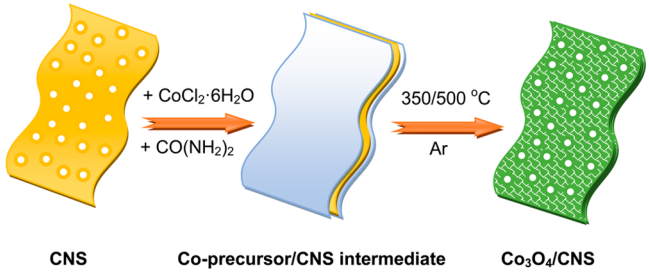

nanosheets are combined based on the following concepts: the high surface area and abundant porosity of carbon nanosheets can provide sufficient anchoring sites for cobalt oxide and ensure fast electrolyte transport; the nanostructured cobalt oxide can short the Li diffusion pathway and enhance the electrochemical properties; and the interconnected carbon nanosheets can be served as high electron transport networks.

Figure 1a shows the XRD patterns of carbon nanosheets, the Co_3O_4/CNS composite, and bare Co_3O_4. The carbon nanosheets shows two significant diffraction peaks centered at 2θ = 22.1 and 43.9° attributed to the (002) and (100) reflections of graphitic carbon, respectively. The intensity ratio of G-band (~1590 cm^{-1}) and D-band (~1340 cm^{-1}) in the Raman spectrum depends on the graphitization degree. The ratio of the integrated intensities (I_G/I_D) for CNS is 0.86 (Figure S2, Supporting Information), which is higher than previously reported commercial activated carbon,[24] confirming the partially ordered graphitic structure of CNS. With the incorporation of cobalt oxide, all the diffraction peaks can be assigned to spinel Co_3O_4 except for the peaks of CNS. This indicates that the synthesized composites are composed of well-crystallized Co_3O_4 and CNS. Compared to that of pure Co_3O_4, the Co_3O_4/CNS composites exhibit broader peak and weaker intensity, suggesting the decoration of nanoscale metal oxide on the surface of carbon nanosheets. As the calcination temperature increased, the peak intensity of the crystalline Co_3O_4 in the composites becomes stronger, suggesting the growth of cobalt oxide nanocrystals.

Growth of Co_3O_4 nanocrystals on CNS was confirmed by TEM for both composites. Figure S3 (in the Supporting Information) highlights the interconnected graphene-like morphology of as-prepared carbon nanosheets. Figure S4 (in the Supporting Information) displays the Co_3O_4/CNS composite layers without finding individual cobalt oxide particles or carbon nanosheets, indicating that a layered structure has been uniformly formed on the surface of carbon nanosheets. Low-resolution TEM images of composited nanosheets exhibit a low contrast, revealing the thin thickness of carbon nanosheets with Co_3O_4 nanocrystal loading (Figure 2a, b). The TEM images shown in Figure 2c, d confirm the uniform distribution of Co_3O_4 nanocrystals. The selected area electron diffraction (SAED) pattern clearly demonstrate the well-textured and crystalline nature of Co_3O_4 nanocrystals in the Co_3O_4/CNS composite. High-resolution TEM images revealed larger particles in Co_3O_4/CNS-500 (~10−20 nm in size) than that in Co_3O_4/CNS-350 (~5 nm in size) (Figure 2e, f), attributed to the rapid growth of cobalt oxide at higher calcination temperature, which is consistent with X-ray diffraction patterns. In addition, the well-resolved periodic lattice fringes with *d* spacings of 0.28 ± 0.01 nm and 0.24 ± 0.01 nm come from the

DOI: 10.1021/am508208c
ACS Appl. Mater. Interfaces 2015, 7, 2882−2890

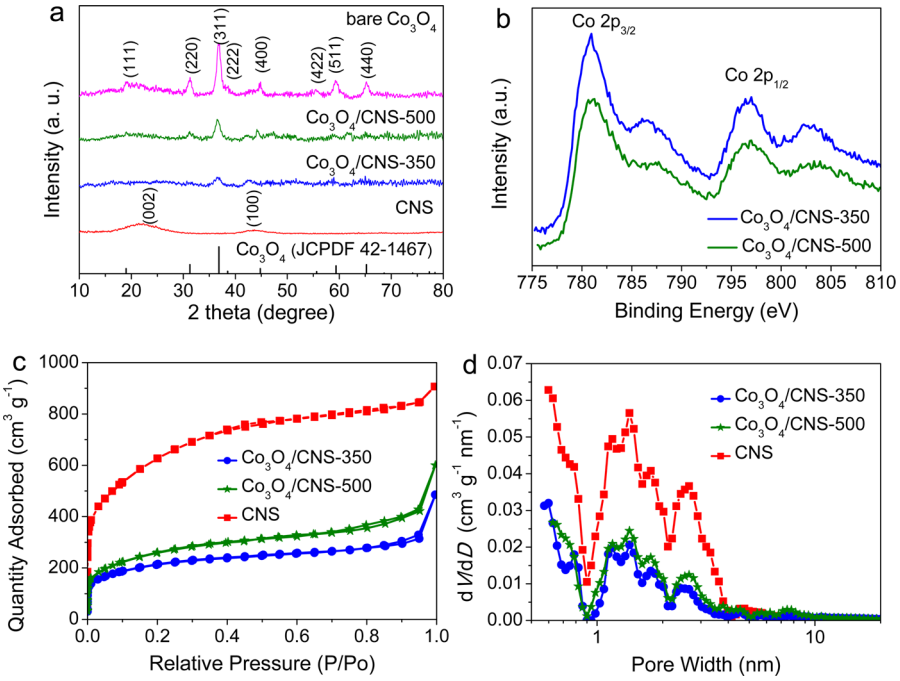

Figure 1. (a) Powder XRD patterns of CNS, Co_3O_4/CNS hybrids, and bare Co_3O_4. (b) Co 2p XPS spectra of Co_3O_4/CNS composites. (c) Nitrogen adsorption−desorption isotherms of CNS and Co_3O_4/CNS. (d) Related pore size distributions, as calculated by density functional theory.

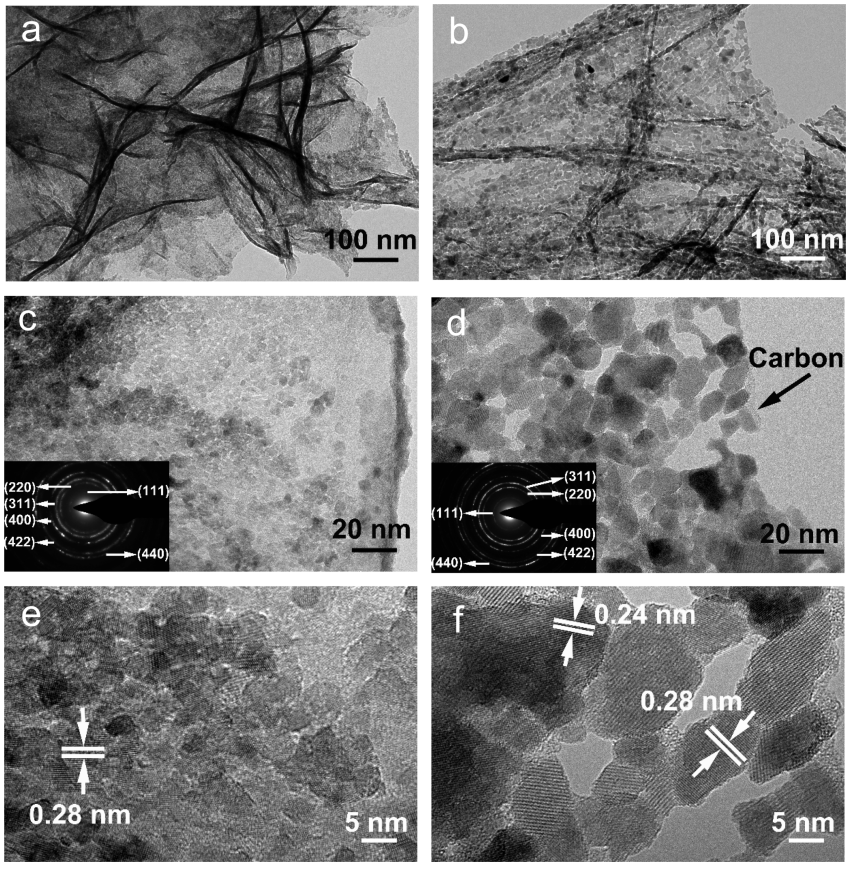

Figure 2. TEM micrographs of Co_3O_4/CNS-350 (a, c, e) and Co_3O_4/CNS-500 (b, d, f): (a, b) low-magnification TEM images, (c, d) bright-field TEM images with inset showing the SAED patterns, (e, f) high-resolution TEM images.

(220) and (311) planes of cubic Co_3O_4. Another phenomenon is that, even after ultrasonication of about 0.5 h to prepare sample for TEM evaluation, the Co_3O_4 nanocrystals are still strongly attached to carbon nanosheets. Therefore, a unique nanoarchitecture of carbon nanosheet-supported Co_3O_4 is readily identified.

DOI: 10.1021/am508208c
ACS Appl. Mater. Interfaces 2015, 7, 2882−2890

To determine the near-surface composition and chemical states of the species in Co_3O_4/CNS composites, we carried out X-ray photoelectron spectroscopy measurements. The Co 2p XPS spectra of the composites exhibit two peaks at 780.9 and 796.4 eV, corresponding to the Co $2p_{3/2}$ and Co $2p_{1/2}$ spin−orbit peaks of cobalt oxide (Figure 1b).[25] The O 1s peak at 530.0 eV associated with the oxygen species in the Co_3O_4 phase confirms the presence of Co_3O_4 in the composite (Figure S5, Supporting Information).[25] Another O 1s peak at ∼532.0 eV is observed, which indicates the existence of residual O^{2-} species (such as −OH and −COOH) boned with C atoms in carbon nanosheets.[26] The C/O atom ratio in carbon nanosheets decreased from 14.3 to 4.3 after nitric acid treatment, and FTIR and XPS techniques confirm the introduction of hydrophilic functional groups (such as −COOH, −C═O, and −OH) on the surface of carbon nanosheets (Figure S6 and S7, Supporting Information).[13] It is noteworthy that the C/O ratio for carbon nanosheets in the Co_3O_4/CNS composites increased to 29.3 and 46.2 after subtracting the oxygen species involved in the formation of Co_3O_4 anchored on the surface of carbon nanosheets. The consumed oxygen-containing groups possibly suggest the strong interaction between carbon nanosheets and Co_3O_4 nanocrystals.[27] Such strong interaction may be the main reason to prevent the agglomeration of nanocrystals to large particles in the presence of carbon nanosheets. Moreover, a high C/O ratio for CNS in the composites indicates that carbon nanosheets are good conductors in comparison to Co_3O_4 nanocrystals, which can serve as a conductive network for efficient electron transport.

The porous nature of Co_3O_4/CNS architectures is demonstrated by the nitrogen adsorption−desorption measurements. The nitrogen adsorption−desorption isotherms and pore size distributions of CNS and Co_3O_4/CNS composites are given in Figure 1c, d. All samples are found to have typical I/IV isotherm curves, indicating a micro/mesoporous structure. The textural parameters of CNS and Co_3O_4/CNS composites are summarized in Table S1 (in the Supporting Information). The calculated Brunauer−Emmett−Teller (BET) specific surface areas decrease from 2260 $m^2\ g^{-1}$ for CNS, to 760 $m^2\ g^{-1}$ for Co_3O_4/CNS-350, and 940 $m^2\ g^{-1}$ for Co_3O_4/CNS-500. The total pore volume also decreases from 1.41 $cm^3\ g^{-1}$ for CNS, to 0.75 $cm^3\ g^{-1}$ for Co_3O_4/CNS-350, and 0.93 $cm^3\ g^{-1}$ for Co_3O_4/CNS-500. It is different from our previous report[13] in that the decrease in the specific surface area and total pore volume with the incorporation of cobalt oxide can be mainly ascribed to the higher density of the composites rather than the pore filling of cobalt oxide.[28] The differences of surface area and pore volume between Co_3O_4/CNS-350 and Co_3O_4/CNS-500 may be related with the different calcination temperature. Higher calcination temperature consumes more oxygen, which would make the blocked pores open. Based on the previous results,[29] pore-filling would significantly reduce the pore size, even at a relatively low loading level of guest materials. In our case, the average pore size of the composites is slightly enlarged from 1.70 nm to 2.16 and 2.43 nm, which can be caused by the presence of a large interconnection void or a void space among the Co_3O_4 nanoparticles. It is clear that the pore size distributions of the composites are similar to that of CNS, indicating the incorporation of cobalt oxide did not occupy or block the space of pores. Thus, the unblocked pores in the carbon nanosheets would ensure fast electrolyte diffusion, and then the surface of metal oxides can be well-soaked in a short time.

Motivated by the advantage of interconnected porous structures in lithium-ion battery, electrochemical tests were performed to evaluate the property of as-synthesized Co_3O_4/CNS composites. Figure 3a, b depicts the first, 10th, 50th, 100th, 200th, and 500th cycle charge−discharge profiles of Co_3O_4/CNS-350 and Co_3O_4/CNS-500 at a current density of 1 A g^{-1} in the potential range from 0.01 to 3 V. It can be seen that the first discharge curve exhibits potential plateaus lower than 1 V, and then shift upward higher than 1 V and become steeper in the subsequent discharge curves, which is similar to previously reported transition metal oxide-based anodes.[30−32] The electrochemical storage mechanism of Co_3O_4 can be described by the electrochemical conversion reaction: $Co_3O_4 + 8Li^+ + 8e^- \leftrightarrow 3Co + 4Li_2O$.[27] The conversion reaction produces a Co phase in a Li_2O matrix as a result of lithiation, whereas the reformation of Co_3O_4 can be occurred during delithiation. The initial reversible capacity is around 730 and 920 mAh g^{-1} for Co_3O_4/CNS-350 and Co_3O_4/CNS-500, respectively (Figure 3c). The Coulombic efficiency for Co_3O_4/CNS-350 rapidly rises from 73% in the first cycle to 99% in the fifth cycle, and then remains above 99% in the following cycles, whereas the initial Coulombic efficiency for Co_3O_4/CNS-500 is 70%, and then increases to above 98% after five cycles (Figure 3d). The large irreversible capacity loss during the first discharge/charge process could be attributed to the decomposition of the electrolyte and the formation of solid electrolyte interphase (SEI) layer.[33] Recent in situ TEM analysis observes an irreversible phase conversion during the first cycle, and the reformation of CoO during delithiation can lead to the capacity fading.[34] Besides, the electronic and structural changes can also result in the irreversible capacity loss.[35] We can notice that a higher Coulombic efficiency is observed in Co_3O_4/CNS-350. The smaller particle size in Co_3O_4/CNS-350 can enhance the electrochemical reactivity,[36] leading to the improvement of Coulombic efficiency. A capacity of about 710 mAh g^{-1} and 970 mAh g^{-1} at 1 A g^{-1} was retained after 500 cycles, which is 97% and 105% of their initial capacities (Figure 3c), indicating the superior cyclability of Co_3O_4/CNS composites.

Besides the excellent cycling performance, the rate capability is also crucial for practical applications of lithium-ion batteries. To investigate the rate capability, the CNS, Co_3O_4/CNS composites, and bare Co_3O_4 anodes were cycled for each ten cycles under an increasing current density of 0.1−10 A g^{-1}, as shown in Figure 3e. The discharge capacities gradually decreased with the increase of the current rate. As we previously demonstrated,[13] CNS exhibits an excellent electrochemical capacity as high as 1320 mAh g^{-1} after the 10th cycle at a current density of 0.1 A g^{-1}, then about 550 mAh g^{-1} after the 40th cycle at 1 A g^{-1}, and about 230 mAh g^{-1} after the 70th cycle at 10 A g^{-1}. After the incorporation of cobalt oxide, the rate performance of Co_3O_4/CNS was greatly improved. For Co_3O_4/CNS-350, the reversible capacity is ∼1100 mAh g^{-1} after the 10th cycle at a current density of 0.1 A g^{-1}, then ∼750 mAh g^{-1} after the 40th cycle at 1 A g^{-1}, and ∼390 mAh g^{-1} after the 70th cycle at 10 A g^{-1}. Importantly, even at a current density of 10 A g^{-1}, the specific capacity of Co_3O_4/CNS-350 is still higher than the theoretical capacity of graphite (372 mAh g^{-1}). Moreover, when the current rate returns from 10 A g^{-1} to the initial 0.1 A g^{-1}, the Co_3O_4/CNS-350 electrode releases a much higher capacity of ∼1230 mAh g^{-1} after the 100th cycle than the initial one. Compared to Co_3O_4/CNS-350, Co_3O_4/CNS-500 exhibits higher specific capacity of ∼1520 mAh g^{-1} at 0.1 A g^{-1} and lower capacity of ∼300 mAh g^{-1} at 10 A g^{-1}. For bare cobalt

DOI: 10.1021/am508208c
ACS Appl. Mater. Interfaces 2015, 7, 2882−2890

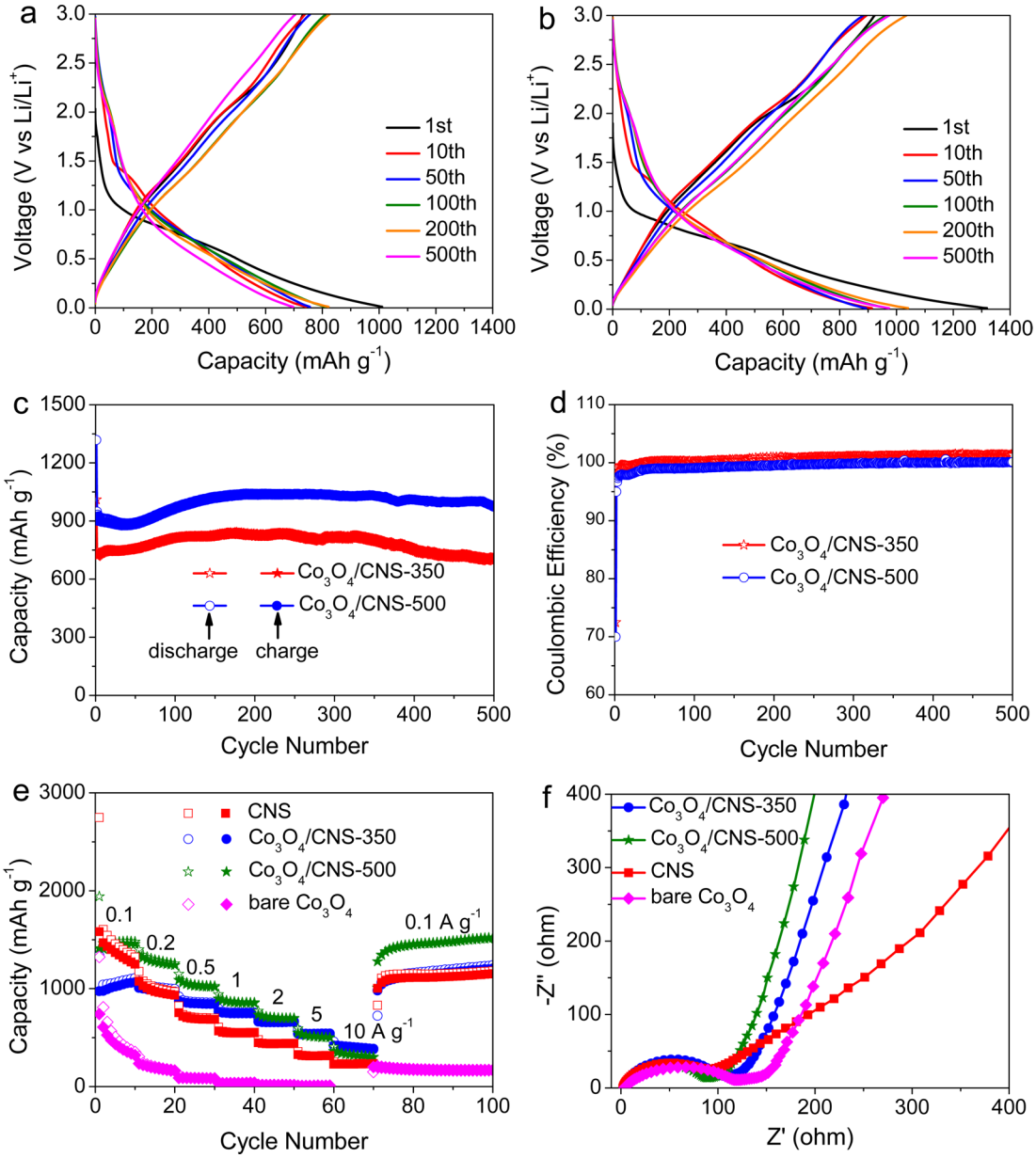

Figure 3. (a) Discharge and charge curves of Co_3O_4/CNS-350 at a current density of 1 A g^{-1}. (b) Discharge and charge curves of Co_3O_4/CNS-500 at a current density of 1 A g^{-1}. (c) Capacity vs. cycle number curves at the current of 1 A g^{-1}. (d) Coulombic efficiency of Co_3O_4/CNS composites during the cycling measurements. (e) Rate capability, at various current densities (hollow: discharge capacity; solid: charge capacity). (f) Nyquist plots of the as-prepared electrodes for CNS, Co_3O_4/CNS-350, Co_3O_4/CNS-500, and bare Co_3O_4.

oxide, the pulverizing effect of cobalt oxide particles during charge/discharge process results in the capacity decreasing drastically,[6,27] and the reversible capacity retains 40 mAh g^{-1} after 40th at a current of 1 A g^{-1}, only maintaining 5% of the initial capacity. Co_3O_4/CNS-350 and Co_3O_4/CNS-500 retain 73% of the initial capacity at the current density of 0.1 A g^{-1}, whereas the initial Coulombic efficiency of CNS and bare cobalt oxide is 58% and 56%, respectively (Figure S8, Supporting Information). It is generally accepted that high surface area of carbon electrode causes heavy formation of SEI layer, which leads to low Coulombic efficiency. For bare Co_3O_4, the irreversible phase conversion can also lead to a capacity fading in the first cycle.[34] The incorporation of Co_3O_4 nanocrystals into porous interconnected carbon framework can achieve lower surface area and the strong interaction between cobalt oxide and carbon nanosheet can reduce the irreversible phase conversion, resulting in the significant improvement of the initial Coulombic efficiency of the hybrids.[34,37] Therefore, the combination of nanosized cobalt oxide and porous carbon nanosheets to form interconnected hybrid is an effective approach to improve the specific capacity and Coulombic efficiency of Co_3O_4.

It is worth noting that the specific capacity of Co_3O_4/CNS hybrids exceeds that of CNS and the theoretical value of Co_3O_4 (890 mAh g^{-1}), indicating a distinguished synergistic effect between CNS and nanosized cobalt oxide.[27,38] Such high capacity can be attributed to the reversible growth of pseudocapacitive polymeric film and the extra lithium adsorption−desorption on the SEI, nanocavities, and/or defects.[6,15] It is accepted that there is a gradual conversion from crystallized metal oxide to amorphous phase during electrochemical measurements, which provides more active sites and/or defects for Li^+ insertion/adsorption,[6,39] and this effect can also lead to

DOI: 10.1021/am508208c
ACS Appl. Mater. Interfaces 2015, 7, 2882−2890

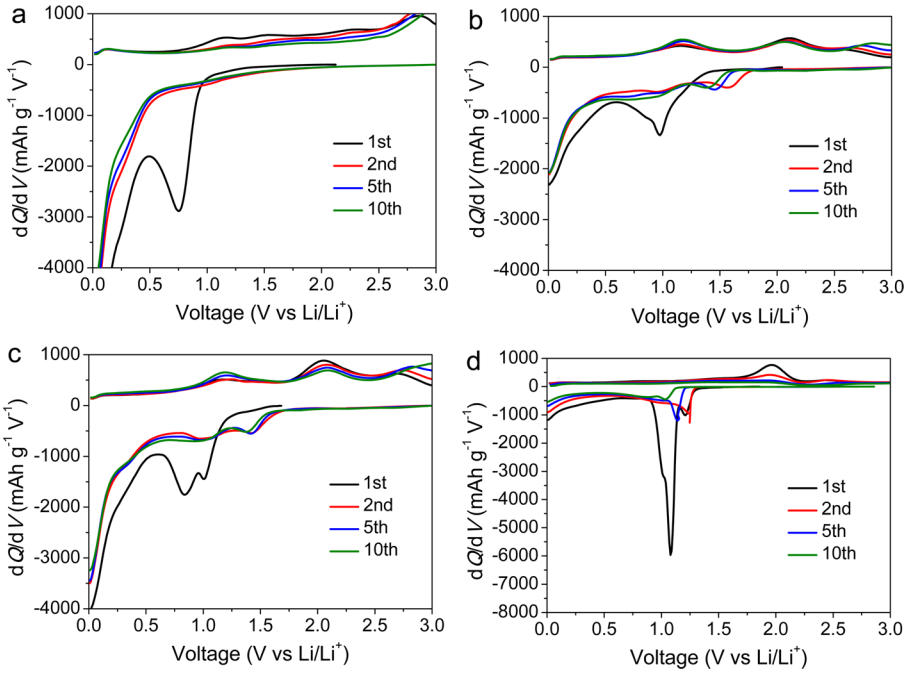

Figure 4. Differential capacity vs. voltage for (a) CNS, (b) Co_3O_4/CNS-350, (c) Co_3O_4/CNS-500, and (d) bare Co_3O_4 during the first, second, fifth, 10th cycles at the current of 0.1 A g^{-1}.

enhanced electrochemical performance for Co_3O_4/CNS hybrids at high rates. Another thing worth emphasizing is the lower value for Co_3O_4/CNS-500 at 10 A g^{-1}. This explanation can be found in the larger particle size in Co_3O_4/CNS-500. The larger particle size in Co_3O_4/CNS-500 could hamper the reactivity for conversion reaction at high rates,[36] leading to higher capacity loss. To emphasize the importance of nanoscale cobalt oxide particles in Co_3O_4/CNS electrodes, the electrochemical impedance spectra (EIS) of as-prepared electrodes were investigated (Figure 3f). Nyquist plots showed that the diameter of the semicircle for Co_3O_4/CNS electrodes in the high-medium frequency region attributed to the charge-transfer reaction at the electrolyte/electrode interface was much smaller than that of bare Co_3O_4 electrodes, suggesting lower contact and charge transfer resistances for composites in the existence of carbon nanosheets.[11,40] The decrease in charge transfer resistance is beneficial for improving the reaction kinetics of the Co_3O_4/CNS hybrid electrode, thus enhancing their electrochemical property. A rough comparison of EIS between Co_3O_4/CNS-350 and Co_3O_4/CNS-500 indicates that Co_3O_4/CNS-350 shows lower total resistance from electrolyte, electrode and separator (Figure S9 and Table S2, Supporting Information), which would help Co_3O_4/CNS-350 electrode to achieve better Coulombic efficiency and rate performance. For Co_3O_4/CNS-500, lower charge-transfer resistance related with the more compact contact between cobalt oxide and carbon nanosheets could be beneficial for higher specific capacity at lower current. The slope of linear part in the low frequency region is related to the diffusion of lithium ions into the bulk electrode. For CNS, the high surface area characteristic could lead to the formation of thick surface film, which prevents the diffusion process.[41] Therefore, the improved diffusion process for Co_3O_4/CNS hybrids may be ascribed to the thinner SEI layer, which would facilitate the diffusion process from or to the electrolyte/electrode.

To better understand the superior electrochemical performance of the hybrid Co_3O_4/CNS electrodes, we plotted dQ/dV (differential capacity) vs. voltage curves at 0.1 A g^{-1} in Figure 4. A plateau in the voltage profile appears as a peak in the differential curve.[42] In the first cycle, an irreversible reduction peak at around 0.75 V for CNS can be associated with electrolyte decomposition and the formation of a SEI layer on the electrode surface. There are two reduction peaks observed at ~0.85 and 1.00 V for the Co_3O_4/CNS composites and at ~1.08 and 1.21 V for bare Co_3O_4 in the first cycle, which are believed to be correspondent with the formation of a SEI layer and the multistep electrochemical reduction reaction of Co^{3+} to Co^{2+} and Co^{2+} to Co. The reduction peaks shifted to ~1.00 and 1.42 V in the following cycles, whereas there is only one obvious reduction peak for bare Co_3O_4, indicating that there will not form Co^{3+} in the reverse reaction process for bare Co_3O_4. The observed anodic peak at ~1.20 and 2.10 V for the Co_3O_4/CNS composites is ascribed to the oxidation process from Li_2O and Co to Co_3O_4. An overlay of the differential capacity curves for Co_3O_4 and CNS demonstrates that the redox reactions in the Co_3O_4/CNS are a composite of the redox process in the underlying carbon and in the Co_3O_4. In addition, the integrated areas of differential capacity vs. voltage curves for Co_3O_4/CNS composites after the initial cycle are much closer than that of bare Co_3O_4, demonstrating better electrochemical reversibility of Co_3O_4/CNS composites, instead of the poor reversibility of bare Co_3O_4.

The Co_3O_4/CNS composites display superior electrochemical capacities and rate capabilities, that are better than or comparable to previously reported nanostructured Co_3O_4 and Co_3O_4/C composites (Table S3, Supporting Information).[14,15,27,30,31,34,37−39,41,43−59] The CNS can serve as interconnected networks to ensure the formation of uniformly dispersed Co_3O_4 nanocrystals. Similarly to graphene, the CNS supports are highly electrically conductive, thus providing an effective and continuous conductive network for fast electron

DOI: 10.1021/am508208c
ACS Appl. Mater. Interfaces 2015, 7, 2882−2890

transportation. Except fast electronic transport, rapid ionic transport is also necessary. Li-ion diffusion is strongly related with the transportation pathway and accessible active sites on the surface of active materials. Shorter path lengths for ionic transport can be achieved with (1) macroscopically open porous nanoarchitectures and (2) nanosized building blocks. Co_3O_4/CNS hybrids with large surface area allows for increased Li^+ flux through the electrode/electrolyte interface, maintaining high charging/discharging rates. Co_3O_4 nanocrystals with fine size can also effectively reduce the solid-state diffusional limitations of Li ions, as the diffusion time (t) is proportional to the square of diffusion length l ($l = (Dt)^{0.5}$, D is the diffusion coefficient[60]). According to the literature, most reported metal oxide/carbon composites including Co_3O_4/CNS-500 have relatively bigger sizes in the range from 10 nm to hundreds of nanometers.[13,61,62] Only a few works reported the synthesis of Co_3O_4/graphene hybrids with particle size of ∼5 nm by using a microwave irradiation method or in situ reduction process.[39,44] By controlling the calcination condition, we successfully coated Co_3O_4 particles with smaller size (∼5 nm) on the surface of low-cost carbon nanosheets by a simple chemical process. It is obvious that Co_3O_4/CNS-350 electrode with smaller particle size exhibits better rate capability, which confirms the advantage of nanosized building blocks. All the above characteristics from the synergistic effect between carbon nanosheets and cobalt oxide nanocrystals make the nanohybrids favorable for fast electronic and ionic transfer, and consequently result in the combination of the highly reversible capacity, superior cyclic performance, and excellent rate capability. We believe that such composite of carbon nanosheet supported with well-dispersed Co_3O_4 nanocrystals is an excellent candidate as anode materials for high-performance lithium-ion batteries.

CONCLUSIONS

We demonstrated that Co_3O_4 nanocrystals were incorporated into porous interconnected carbon framework assembled by carbon nanosheets through a facile chemical route for high-performance battery materials. The Co_3O_4 nanocrystals held a diameter down to 5 nm and uniform dispersity on the carbon nanosheets. The designed hybrid networks inherit the advantages of nanosized cobalt oxide and interconnected carbon nanosheets. Nanostructured Co_3O_4 particles homogeneously anchored on carbon nanosheets can improve the initial Coulombic efficiency and provide short path length for Li^+ transport to facilitate the lithium diffusion kinetics. Meanwhile, carbon nanosheets act as conductive supports for the enhancement of electron transport. As a result, such a composite with strong interaction between Co_3O_4 nanocsystals and carbon nanosheets is capable of achieving high reversible specific capacitiy (>1200 mAh g^{-1} at 0.1 A g^{-1}), excellent cyclic performance (capacity retention of 97/105% after 500 cycles), and superior rate capability (∼390 mAh g^{-1} at 10 A g^{-1}). In addition, the used carbon nanosheets in the present work show obvious advantageous than graphene materials based on their intrinsic characteristics of interconnected structure, cost-effective, and easy manipulation. We believe that carbon nanosheets can be used as an excellent substitute for graphene materials and such high performance carbon-nanosheet-based hybrids can offer great promise in large-scale energy-storage device applications.

ASSOCIATED CONTENT

Supporting Information

Thermogravimetric curves of Co_3O_4/CNS-350, Raman spectra of CNS and Co_3O_4/CNS, SEM images of CNS and Co_3O_4/CNS, O 1s XPS spectra of Co_3O_4/CNS composites, FTIR and XPS spectra of CNS and nitric-acid-treated CNS, Nyquist plots of Co_3O_4/CNS composites, physical parameters for CNS and Co_3O_4/CNS composites, a comparison table with literature of the reversible capacities of cobalt oxide-based materials, and kinetic parameters for CNS, Co_3O_4/CNS-350, Co_3O_4/CNS-500, and bare Co_3O_4 electrodes. This material is available free of charge via the Internet at http://pubs.acs.org.

AUTHOR INFORMATION

Corresponding Authors

*E-mail: huanleiwang@gmail.com.
*E-mail: wangxinhd@ouc.edu.cn.

Notes

The authors declare no competing financial interest.

ACKNOWLEDGMENTS

This work was funded by National Natural Science Foundation of China (51402272, and 21471139), China Postdoctoral Science Foundation (2014M560581), Shandong Province Outstanding Youth Scientist Foundation Plan (BS2014CL024), Seed Fund from Ocean University of China, and Fundamental Research Funds for the Central Universities.

REFERENCES

(1) Dunn, B.; Kamath, H.; Tarascon, J. M. Electrical Energy Storage for the Grid: A Battery of Choices. *Science* **2011**, *334*, 928−935.
(2) Bruce, P. G.; Scrosati, B.; Tarascon, J. M. Nanomaterials for Rechargeable Lithium Batteries. *Angew. Chem., Int. Ed.* **2008**, *47*, 2930−2946.
(3) Liu, C.; Li, F.; Ma, L. P.; Cheng, H. M. Advanced Materials for Energy Storage. *Adv. Mater.* **2010**, *22*, E28−E62.
(4) Reddy, M. V.; Rao, G. V. S.; Chowdari, B. V. R. Metal Oxides and Oxysalts as Anode Materials for Li Ion Batteries. *Chem. Rev.* **2013**, *113*, 5364−5457.
(5) Stephenson, T.; Li, Z.; Olsen, B.; Mitlin, D. Lithium Ion Battery Applications of Molybdenum Disulfide (MoS_2) Nanocomposites. *Energy Environ. Sci.* **2014**, *7*, 209−231.
(6) Peng, C. X.; Chen, B. D.; Qin, Y.; Yang, S. H.; Li, C. Z.; Zuo, Y. H.; Liu, S. Y.; Yang, J. H. Facile Ultrasonic Synthesis of CoO Quantum Dot/Graphene Nanosheet Composites with High Lithium Storage Capacity. *ACS Nano* **2012**, *6*, 1074−1081.
(7) Sun, Y. M.; Hu, X. L.; Luo, W.; Xia, F. F.; Huang, Y. H. Reconstruction of Conformal Nanoscale MnO on Graphene as a High-Capacity and Long-Life Anode Materials for Lithium Ion Batteries. *Adv. Funct. Mater.* **2013**, *23*, 2436−2444.
(8) Jiang, H.; Hu, Y. J.; Guo, S. J.; Yan, C. Y.; Lee, P. S.; Li, C. Z. Rational Design of MnO/Carbon Nanopeapods with Internal Void Space for High-Rate and Long-Life Li-Ion Batteries. *ACS Nano* **2014**, *8*, 6038−6046.
(9) Su, Y. Z.; Li, S.; Wu, D. Q.; Zhang, F.; Liang, H. W.; Gao, P. F.; Cheng, C.; Feng, X. L. Two-Dimensional Carbon-Coated Graphene/Metal Oxide Hybrids for Enhanced Lithium Storage. *ACS Nano* **2012**, *6*, 8349−8356.
(10) Fei, H. L.; Peng, Z. W.; Li, L.; Yang, Y.; Lu, W.; Samuel, E. L. G.; Fan, X. J.; Tour, J. M. Preparation of Carbon-Coated Iron Oxide Nanoparticles Dispersed on Graphene Sheets and Applications as Advanced Anode Materials for Lithium-Ion Batteries. *Nano Res.* **2014**, *7*, 502−510.

DOI: 10.1021/am508208c
ACS Appl. Mater. Interfaces 2015, 7, 2882−2890

(11) Yin, L. W.; Zhang, Z. W.; Li, Z. Q.; Hao, F. B.; Li, Q.; Wang, C. X.; Fan, R. H.; Qi, Y. X. Spinel $ZnMn_2O_4$ Nanocrystal-Anchored 3D Hierarchical Carbon Aerogel Hybrids as Anode Materials for Lithium Ion Batteries. *Adv. Funct. Mater.* **2014**, *24*, 4176−4185.
(12) Gong, Y. J.; Yang, S. B.; Liu, Z.; Ma, L. L.; Vajtai, R.; Ajayan, P. M. Graphene-Network-Backboned Architectures for High-Performance Lithium Storage. *Adv. Mater.* **2013**, *25*, 3979−3984.
(13) Wang, H. L.; Xu, Z. W.; Li, Z.; Cui, K.; Ding, J.; Kohandehghan, A.; Tan, X. H.; Zahiri, B.; Olsen, B. C.; Holt, C. M. B.; Mitlin, D. Hybrid Device Employing Three-Dimensional Arrays of MnO in Carbon Nanosheets Bridges Battery-Supercapacitor Divide. *Nano Lett.* **2014**, *14*, 1987−1994.
(14) Abouali, S.; Garakani, M.; Zhang, B.; Luo, H.; Xu, Z. L.; Huang, J. Q.; Huang, J. Q.; Kim, J. K. Co_3O_4/Porous Electrospun Carbon Nanofibers as Anodes for High Performance Li-Ion Batteries. *J. Mater. Chem. A* **2014**, *2*, 16939−16944.
(15) Ryu, W. H.; Shin, J.; Jung, J. W.; Kim, I. D. Cobalt(II) Monoxide Nanoparticles Embedded in Porous Carbon Nanofibers as a Highly Reversible Conversion Reaction Anode for Li-Ion Batteries. *J. Mater. Chem. A* **2013**, *1*, 3239−3243.
(16) Lee, S. H.; Sridhar, V.; Jung, J. H.; Karthikeyan, K.; Lee, Y. S.; Mukherjee, R.; Koratkar, N.; Oh, I. K. Graphene-Nanotube-Iron Hierarchical Nanostructure as Lithium Ion Battery Anode. *ACS Nano* **2013**, *7*, 4242−4251.
(17) Hou, X. Y.; Jiang, H.; Hu, Y. J.; Li, Y. F.; Hu, J. C.; Li, C. Z. In Situ Deposition of Hierarchical Architecture Assembly from Sn-Filled CNTs for Lithium-Ion Batteries. *ACS Appl. Mater. Interfaces* **2013**, *5*, 6672−6677.
(18) Guo, C. X.; Wang, M.; Chen, T.; Lou, X. W.; Li, C. M. A Herarchically Nanostructured Composite of MnO_2/Conjugated Polymer/Graphene for High-Performance Lithium Ion Batteries. *Adv. Energy Mater.* **2011**, *1*, 736−741.
(19) Wang, H. L.; Liang, Y. Y.; Mirfakhrai, T.; Chen, Z.; Casalongue, H. S.; Dai, H. J. Advanced Asymmetrical Supercapacitors Based on Graphene Hybrid Materials. *Nano Res.* **2011**, *4*, 729−736.
(20) Chang, H. X.; Wu, H. K. Graphene-Based Nanocomposites: Preparation, Functionalization, and Energy and Environmental Applications. *Energy Environ. Sci.* **2013**, *6*, 3483−3507.
(21) Gu, Y.; Xu, Y.; Wang, Y. Graphene-Wrapped CoS Nanoparticles for High-Capacity Lithium-Ion Storage. *ACS Appl. Mater. Interfaces* **2013**, *5*, 801−806.
(22) Wang, H.; Xu, Z. W.; Kohandehghan, A.; Li, Z.; Cui, K.; Tan, X. H.; Stephenson, T. J.; King'ondu, C. K.; Holt, C. M. B.; Olsen, B. C.; Tak, J. K.; Harfield, D.; Anyia, A. O.; Mitlin, D. Interconnected Carbon Nanosheets Derived from Hemp for Ultrafast Supercapacitors with High Energy. *ACS Nano* **2013**, *7*, 5131−5141.
(23) Wang, H. L.; Holt, C. M. B.; Li, Z.; Tan, X. H.; Amirkhiz, B. S.; Xu, Z. W.; Olsen, B. C.; Stephenson, T.; Mitlin, D. Graphene-Nickel Cobaltite Nanocomposite Asymmetrical Supercapacitor with Commercial Level Mass Loading. *Nano Res.* **2012**, *5*, 605−617.
(24) Ding, J.; Wang, H. L.; Li, Z.; Kohandehghan, A.; Cui, K.; Xu, Z. W.; Zahiri, B.; Tan, X. H.; Lotfabad, E. M.; Olsen, B. C.; Mitlin, D. Carbon Nanosheet Frameworks Derived from Peat Moss as High Performance Sodium Ion Battery Anodes. *ACS Nano* **2013**, *7*, 11004−11015.
(25) Varghese, B.; Hoong, T. C.; Yanwu, Z.; Reddy, M. V.; Chowdari, B. V. R.; Wee, A. T. S.; Vincent, T. B. C.; Lim, C. T.; Sow, C. H. Co_3O_4 Nanostructures with Different Morphologies and Their Field-Emission Properties. *Adv. Funct. Mater.* **2007**, *17*, 1932−1939.
(26) Schniepp, H. C.; Li, J. L.; McAllister, M. J.; Sai, H.; Herrera-Alonso, M.; Adamson, D. H.; Prud'homme, R. K.; Car, R.; Saville, D. A.; Aksay, I. A. Functionalized Single Graphene Sheets Derived from Splitting Graphite Oxide. *J. Phys. Chem. B* **2006**, *110*, 8535−8539.
(27) Wu, Z. S.; Ren, W. C.; Wen, L.; Gao, L. B.; Zhao, J. P.; Chen, Z. P.; Zhou, G. M.; Li, F.; Cheng, H. M. Graphene Anchored with Co_3O_4 Nanoparticles as Anode of Lithium Ion Batteries with Enhanced Reversible Capacity and Cyclic Performance. *ACS Nano* **2010**, *4*, 3187−3194.
(28) Zhao, X.; Zhang, L. L.; Murali, S.; Stoller, M. D.; Zhang, Q. H.; Zhu, Y. W.; Ruoff, R. S. Incorporation of Manganese Dioxide within Ultraporous Activated Graphene for High-Performance Electrochemical Capacitors. *ACS Nano* **2012**, *6*, 5404−5412.
(29) Li, L.; Shi, J. L.; Zhang, L. X.; Xiong, L. M.; Yan, J. N. A Novel and Simple In-Situ Reduction Route for the Synthesis of an Ultra-Thin Metal Nanocoating in the Channels of Mesoporous Silica Materials. *Adv. Mater.* **2004**, *16*, 1079−1082.
(30) Wu, R. B.; Qian, X. K.; Zhou, K.; Wei, J.; Lou, J.; Ajayan, P. M. Porous Spinel $Zn_xCo_{3-x}O_4$ Hollow Polyhedra Templated for High-Rate Lithium-Ion Batteries. *ACS Nano* **2014**, *8*, 6297−6303.
(31) Lai, L. F.; Zhu, J. X.; Li, Z. G.; Yu, D. Y. W.; Jiang, S. R.; Cai, X. Y.; Yan, Q. Y.; Lam, Y. M.; Shen, Z. X.; Lin, J. Y. Co_3O_4/Nitrogen Modified Graphene Electrode as Li-Ion Battery Anode with High Reversible Capacity and Improved Initial Cycle Performance. *Nano Energy* **2014**, *3*, 134−143.
(32) Chen, Y.; Song, B. H.; Li, M.; Lu, L.; Xue, J. M. Fe_3O_4 Nanoparticles Embedded in Uniform Mesoporous Carbon Spheres for Superior High-Rate Battery Applications. *Adv. Funct. Mater.* **2014**, *24*, 319−326.
(33) Laruelle, S.; Grugeon, S.; Poizot, P.; Dolle, M.; Dupont, L.; Tarascon, J. M. On the Origin of the Extra Electrochemical Capacity Displayed by MO/Li Cells at Low Potential. *J. Electrochem. Soc.* **2002**, *149*, A627−A634.
(34) Su, Q. M.; Zhang, J.; Wu, Y. S.; Du, G. H. Revealing the Electrochemical Conversion Mechanism of Porous Co_3O_4 Nanoplates in Lithium Ion Battery by In Situ Transmission Electron Microscopy. *Nano Energy* **2014**, *9*, 264−272.
(35) Kim, Y.; Lee, J. H.; Cho, S.; Kwon, Y.; In, I.; Lee, J.; You, N. H.; Reichmanis, E.; Ko, H.; Lee, K. T.; Kwon, H. K.; Ko, D. H.; Yang, H.; Park, B. Additive-Free Hollow-Structured Co_3O_4 Nanoparticle Li-Ion Battery: the Origins of Irreversible Capacity Loss. *ACS Nano* **2014**, *8*, 6701−6712.
(36) Poizot, P.; Laruelle, S.; Grugeon, S.; Dupont, L.; Tarascon, J. M. Nano-Sized Transition-Metal Oxides as Negative-Electrode Materials for Lithium-Ion Batteries. *Nature* **2000**, *407*, 496−499.
(37) Zhu, X.; Ning, G. Q.; Ma, X. L.; Fan, Z. J.; Xu, C. G.; Gao, J. S.; Xu, C. M.; Wei, F. High Density Co_3O_4 Nanoparticles Confined in a Porous Graphene Nanomesh Network Driven by an Electrochemical Process: Ultra-High Capacity and Rate Performance for Lithium Ion Batteries. *J. Mater. Chem. A* **2013**, *1*, 14023−14030.
(38) Qiang, S.; Chen, Q.; Wang, Y. Microwave-Assisted Synthesis of a Co_3O_4-Graphene Sheet-on-Sheet Nanocomposite as a Superrior Anode Material for Li-Ion Batteries. *J. Mater. Chem.* **2010**, *20*, 9735−9739.
(39) Zhou, X. Y.; Shi, J. J.; Liu, Y.; Su, Q. M.; Zhang, J.; Du, G. H. Microwave Irradiation Synthesis of Co_3O_4 Quantum Dots/Graphene Composite as Anode Materials for Li-Ion Battery. *Electrochim. Acta* **2014**, *143*, 175−179.
(40) Zhang, K. J.; Han, P. X.; Gu, L.; Zhang, L. X.; Liu, Z. H.; Kong, Q. S.; Zhang, C. J.; Dong, S. M.; Zhang, Z. Y.; Yao, J. H.; Xu, H. X.; Cui, G. L.; Chen, L. Q. Synthesis of nitrogen-doped MnO/graphene nanosheets hybrid material for lithium ion batteries. *ACS Appl. Mater. Interfaces* **2012**, *4*, 658−664.
(41) Hsieh, C. T.; Lin, J. S.; Chen, Y. F.; Teng, H. S. Pulse Microwave Deposition of Cobalt Oxide Nanoparticles on Graphene Nanosheets as Anode Materials for Lithium Ion Batteries. *J. Phys. Chem. C* **2012**, *116*, 15251−15258.
(42) Wu, G. T.; Wang, C. S.; Zhang, X. B.; Yang, H. S.; Qi, Z. F.; He, P. M.; Li, W. Z. Structure and Lithium Insertion Properties of Carbon Nanotubes. *J. Electrochem. Soc.* **1999**, *146*, 1696−1701.
(43) Yang, X. L.; Fan, K. C.; Zhu, Y. H.; Shen, J. H.; Jiang, X.; Zhao, P.; Li, C. Z. Tailored Graphene-Encapsulated Mesoporous Co_3O_4 Composite Microspheres for High-Performance Lithium Ion Batteries. *J. Mater. Chem.* **2012**, *22*, 17278−17283.
(44) Kim, H.; Seo, D. H.; Kim, S. W.; Kim, J.; Kang, K. Highly Reversible Co_3O_4/Graphene Hybrid Anode for Lithium Rechargeable Batteries. *Carbon* **2011**, *49*, 326−332.

DOI: 10.1021/am508208c
ACS Appl. Mater. Interfaces 2015, 7, 2882−2890

(45) Sun, H. T.; Sun, X.; Hu, T.; Yu, M. P.; Lu, F. Y.; Lian, J. Graphene-Wrapped Mesoporous Cobalt Oxide Hollow Spheres Anode for High-Rate and Long-Life Lithium Ion Batteries. *J. Phys. Chem. C* **2014**, *118*, 2263−2272.
(46) Yang, X. L.; Fan, K. C.; Zhu, Y. H.; Shen, J. H.; Jiang, X.; Zhao, P.; Luan, S. R.; Li, C. Z. Electric Papers of Graphene-Coated Co_3O_4 Fibers for High-Performance Lithium-Ion Batteries. *ACS Appl. Mater. Interfaces* **2013**, *5*, 997−1002.
(47) Garakani, M. A.; Abouali, S.; Zhang, B.; Takagi, C. A.; Xu, Z. L.; Huang, J. Q.; Huang, J.; Kim, J. K. Cobalt Carbonate/ and Cobalt Oxide/Graphene Aerogel Composite Anodes for High Performance Li-Ion Batteries. *ACS Appl. Mater. Interfaces* **2014**, *6*, 18971−18980.
(48) Anh, L. T.; Rai, A. K.; Thi, T. V.; Gim, J.; Kim, S.; Mathew, V.; Kim, J. Enhanced Electrochemical Performance of Novel K-Doped Co_3O_4 as the Anode Material for Secondary Lithium-Ion Batteries. *J. Mater. Chem. A* **2014**, *2*, 6966−6975.
(49) Li, L.; Seng, K. H.; Chen, Z. X.; Guo, Z. P.; Liu, H. K. Self-Assembly of Hierarchical Star-Like Co_3O_4 Micro/Nanostructures and Their Application in Lithium Ion Batteries. *Nanoscale* **2013**, *5*, 1922−1928.
(50) Wang, J. Y.; Yang, N. L.; Tang, H. J.; Dong, Z. H.; Jin, Q.; Yang, M.; Kisailus, D.; Zhao, H. J.; Tang, Z. Y.; Wang, D. Accurate Control of Multishelled Co_3O_4 Hollow Microspheres as High-Performance Anode Materials in Lithium-Ion Batteries. *Angew. Chem., Int. Ed.* **2013**, *52*, 6417−6420.
(51) Sun, H. Y.; Liu, Y. G.; Yu, Y. L.; Ahmad, M.; Nan, D.; Zhu, J. Mesoporous Co_3O_4 Nanosheets-3D Graphene Networks Hybrid Materials for High-Performance Lithium Ion Batteries. *Electrochim. Acta* **2014**, *118*, 1−9.
(52) Liang, C. C.; Cheng, D. F.; Ding, S. J.; Zhao, P. F.; Zhao, M. S.; Song, X. P.; Wang, F. The Structure Dependent Electrochemical Performance of Porous Co_3O_4 Nanoplates as Anode Materials for Lithium-Ion Batteries. *J. Power Sources* **2014**, *251*, 351−356.
(53) Li, L.; Zhou, G. M.; Shan, X. Y.; Pei, S. F.; Li, F.; Cheng, H. M. Co_3O_4 Mesoporous Nanostructures@Graphene Membrane as an Integrated Anode for Long-Life Lithium-Ion Batteries. *J. Power Sources* **2014**, *255*, 52−58.
(54) Zhan, L.; Wang, S. Q.; Ding, L. X.; Li, Z.; Wang, H. H. Grass-Like Co_3O_4 Nanowire Arrays Anode with High Rate Capability and Excellent Cycling Stability for Lithium-Ion Batteries. *Electrochim. Acta* **2014**, *135*, 35−41.
(55) Ge, D. H.; Geng, H. B.; Wang, J. Q.; Zheng, J. W.; Pan, Y.; Cao, X. Q.; Gu, H. W. Porous Nano-Structured Co_3O_4 Anode Materials Generated from Coordination-Driven Self-Assembled Aggregates for Advanced Lithium Ion Batteries. *Nanoscale* **2014**, *6*, 9689−9694.
(56) Huang, G. Y.; Xu, S. M.; Lu, S. S.; Li, L. Y.; Sun, H. Y. Micro/Nanostructured Co_3O_4 Anode with Enhanced Rate Capability for Lithium-Ion Batteries. *ACS Appl. Mater. Interfaces* **2014**, *6*, 7236−7243.
(57) Hao, F. B.; Zhang, Z. W.; Yin, L. W. Co_3O_4/Carbon Aerogel Hybrids as Anode Materials for Lithium-Ion Batteries with Enhanced Electrochemical Properties. *ACS Appl. Mater. Interfaces* **2013**, *5*, 8337−8344.
(58) Wang, L.; Zheng, Y. L.; Wang, X. H.; Shen, S. H.; Xu, F. G.; Zu, L.; Wu, J. F.; Sun, L. L.; Li, Z.; Hou, H. Q.; Song, Y. H. Nitrogen-Doped Porous Carbon/Co_3O_4 Nanocomposites as Anode Materials for Lithium-Ion Batteries. *ACS Appl. Mater. Interfaces* **2014**, *6*, 7117−7125.
(59) Wu, F. D.; Wang, Y. Self-Assembled Echinus-Like Nanostructures of Mesoporous CoO Nanorod/CNT for Lithium-Ion Batteries. *J. Mater. Chem.* **2011**, *21*, 6636−6641.
(60) Wang, D. W.; Li, F.; Liu, M.; Lu, G. Q.; Cheng, H. M. Mesopore-Aspect-Ratio Dependence of Ion Transport in Rodtype Ordered Mesoporous Carbon. *J. Phys. Chem. C* **2008**, *112*, 9950−9955.
(61) Liang, Y. Y.; Li, Y. G.; Wang, H. L.; Zhou, J. G.; Wang, J.; Regier, T.; Dai, H. J. Co_3O_4 Nanocrystals on Graphene as a Synergistic Catalyst for Oxygen Reduction Reaction. *Nat. Mater.* **2011**, *10*, 780−786.
(62) Zhou, G. M.; Wang, D. W.; Yin, L. C.; Li, N.; Li, F.; Cheng, H. M. Oxygen Bridges Between NiO Nanosheets and Graphene for Improvement of Lithium Storage. *ACS Nano* **2012**, *6*, 3214−3223.

DOI: 10.1021/am508208c
ACS Appl. Mater. Interfaces 2015, 7, 2882−2890